ACS APPLIED MATERIALS & INTERFACES

www.acsami.org

Research Article

Inhibition of Tumor–Host Cell Interactions Using Synthetic Heparin Mimetics

Lukas M. Gockel, Martin Heyes, Honglian Li, Abdullah Al Nahain, Christian Gorzelanny, Martin Schlesinger, Stefan Holdenrieder, Jin-Ping Li, Vito Ferro, and Gerd Bendas*

Cite This: *ACS Appl. Mater. Interfaces* 2021, 13, 7080–7093

Read Online

ACCESS | Metrics & More | Article Recommendations | Supporting Information

ABSTRACT: Low-molecular-weight heparin (LMWH) is the guideline-based drug for antithrombotic treatment of cancer patients, while its direct antitumor effects are a matter of ongoing debate. Although therapeutically established for decades, LMWH has several drawbacks mainly associated with its origin from animal sources. Aiming to overcome these limitations, a library of synthetic heparin mimetic polymers consisting of homo- and copolymers of sulfonated and carboxylated noncarbohydrate monomers has recently been synthesized via reversible addition–fragmentation chain transfer polymerization. These heparin mimetics were investigated for their capacities to interfere with simulated steps of tumor cell metastasis. Among them, homo- and copolymers from sodium 4-styrenesulfonate (poly(SSS)) with acrylic acid (poly(SSS-*co*-AA)) with an MW between 5 and 50 kDa efficiently attenuated cancer cell-induced coagulation and thus platelet activation and degranulation similar to or even better than LMWH. Furthermore, independent of anticoagulant activities, these polymers affected other metastasis-relevant targets with impressive affinities. Hence, they blocked heparanase enzymatic activity outmatching commercial heparins or a glycosidic drug candidate. Furthermore, these polymers bind P-selectin and the integrin VLA-4 similar to or even better than heparin, indicated by a biosensor approach and thus efficiently blocked melanoma cell binding to endothelium under blood flow conditions. This is the first report on the prospects of synthetic heparin mimetics as promising nontoxic compounds in oncology to potentially substitute heparin as an anticoagulant and to better understand its role as an antimetastatic drug.

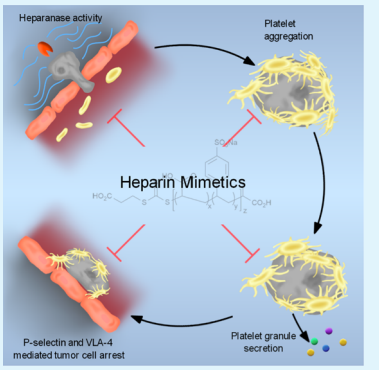

KEYWORDS: *cancer, heparanase, heparin mimetics, metastasis, platelets, VLA-4, VCAM-1, P-selectin*

INTRODUCTION

Despite tremendous achievements in the early diagnosis of cancer and development of innovative treatment therapies to interfere with progression of tumors, malignant neoplasms rank behind cardiovascular diseases as the second leading cause of deaths in Europe and the US.[1] This discrepancy of treatment progress on the one hand and still stagnating mortality rates on the other hand are, among various factors, related to tumor metastasis, which is considered a major reason for cancer-related death.[2] Hematogenous metastatic spread of tumors is a highly orchestrated process, which is mediated by a crosstalk of tumor cells with the microenvironment, various host cell populations, and explicitly in the phase of hematogenous distribution, with soluble or cellular blood components. However, no antimetastatic pharmacological strategy is becoming apparent presently.

The development of thrombotic events is related to another significant complication that strongly correlates with metastatic cancer progression and fatal outcome. This comprises most likely venous thromboembolism (VTE), such as deep venous thrombosis or pulmonary embolism, but also arterial thrombosis.[3,4] This relationship between thrombosis and cancer is mechanistically complex, affected by physical and cellular effects and known since the 19th century, referred to as Trousseau syndrome.[5] The incidence of cancer-related VTE varies by tumor-related factors, such as tumor entity and stage, by patient-individual factors and also by cytostatic or other treatment factors.[6,7] However, about 15% of cancer patients will develop VTE. Notably, the development of VTE reduces the 1-year survival of cancer patients to roughly one-third of the survival rate of cancer patients that did not develop VTE. Thus, VTE complications represent the second leading cause of death in these patients.[8,9]

Consequently, an antithrombotic prophylaxis and treatment is an essential component in clinical oncology, especially for certain risk patient populations and treatment regimes. A still open issue refers to the question whether VTE treatment has

Received: November 20, 2020
Accepted: January 25, 2021
Published: February 3, 2021

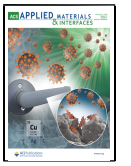

https://doi.org/10.1021/acsami.0c20744
ACS Appl. Mater. Interfaces 2021, 13, 7080–7093

Table 1. Structures of Evaluated Heparin-Mimicking Polymers and Their Performance in LTA Screening to Assess Inhibition of Cancer Cell-Induced Platelet Aggregation in Platelet-Rich Buffer[a]

Polymer	Structure	LTA	Polymer	Structure	LTA
Poly(SSS)	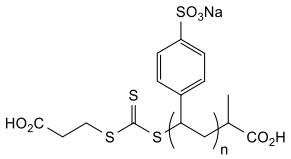	+	Poly(AMPS-*co*-AA)	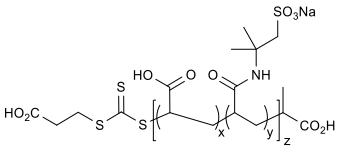	--
Poly(SPA)	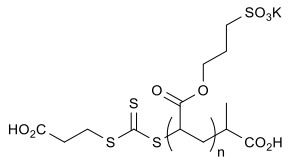	--	Poly(SSS-*co*-SPA)	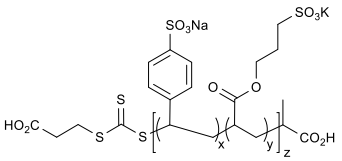	+
Poly(SPM)	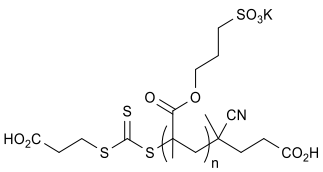	--	Poly(SSS-*co*-SPM)	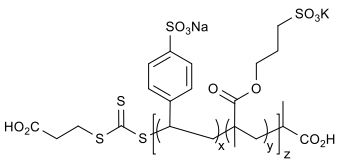	+
Poly(AMPS)	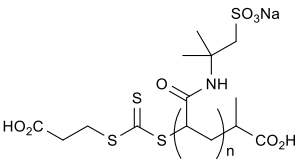	-	Poly(SSS-*co*-AMPS)	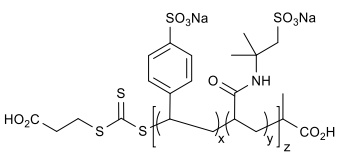	+
Poly(AA)	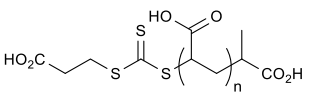	--	Poly(SPA-*co*-SPM)	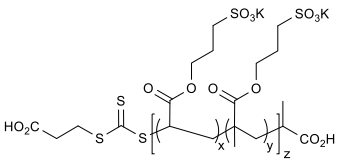	--
Poly(SSS-*co*-AA)	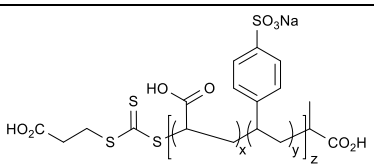	++	Poly(SPA-*co*-AMPS)	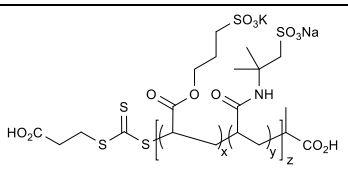	--
Poly(SPA-*co*-AA)	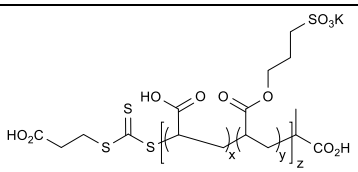	--	Poly(SPM-*co*-AMPS)	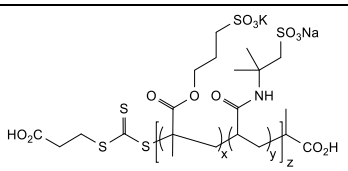	--
Poly(SPM-*co*-AA)	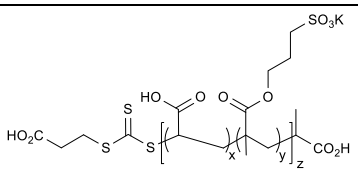	--			

[a]See also Figure S1 and Table S1. All polymers posses low dispersities with $Đ$ in the range 1.08−1.38, detected by GPC.[29,30] Moderate inhibitory effects were indicated by "+", stronger inhibition by "++", whereas "−" or "--" indicated no inhibitory capacity.

an effect on cancer progression, most likely the metastatic spread of tumors. The treatment guidelines of first-line therapy for the short- and long-term management of cancer-associated VTE, including those of the European Society of Medical Oncology (ESMO) or the American Society of Clinical Oncology (ASCO), currently recommend low-molecular-weight heparin (LMWH) as the drug of choice.[10] Some clinical trials indicated a survival benefit for patients receiving LMWH as VTE prophylaxis, while others failed to show this. Thus, the question remains open whether LMWH treatment is beneficial for cancer patients exceeding solely its antithrombotic effects.[11,12] During the last two decades, there was

https://doi.org/10.1021/acsami.0c20744
ACS Appl. Mater. Interfaces 2021, 13, 7080−7093

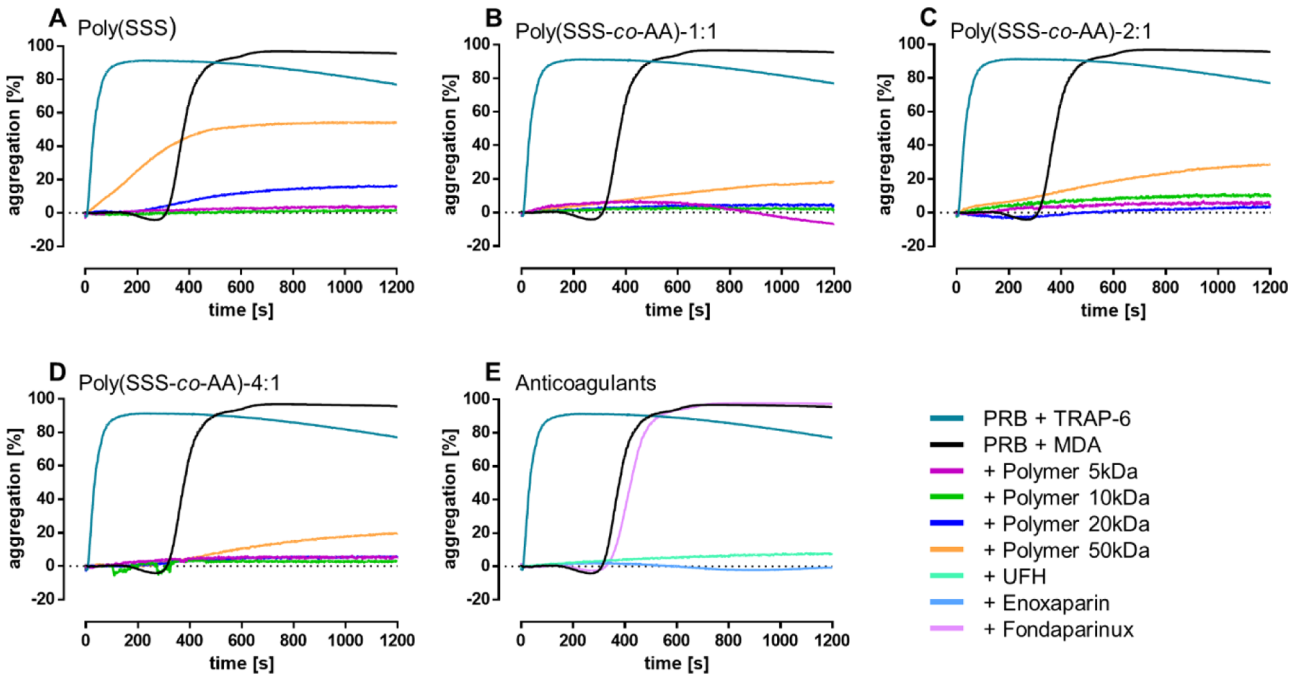

Figure 1. Heparin-mimicking polymers impair tumor cell-induced platelet aggregation. Representative curves of MDA-MB-231 cell-induced platelet aggregation in platelet-rich buffer (PRB) are shown. Platelets were incubated with (A) poly(SSS), (B) poly(SSS-*co*-AA)-1:1, (C) poly(SSS-*co*-AA)-2:1, and (D) poly(SSS-*co*-AA)-4:1 of varying size at a concentration of 50 μg/mL. (E) For comparison, platelets were preincubated with the adopted therapeutic concentrations of commercially available heparins, UFH (1 IU/mL), enoxaparin (1 IU/mL), and the anticoagulant fondaparinux (775 ng/mL) prior to tumor cell activation.

significant interest in preclinical research to identify potential target structures of LMWH for interference with the metastatic tumor spread. Adhesion receptors, such as selectins,[13] integrins,[14,15] the enzyme heparanase,[16] or other probable targets of heparin, were identified,[17] which partly led to the clinical development of heparin-based inhibitors.[18] One of the key events in the metastatic dissemination of cancer cells in the blood is the activation of and interaction with platelets. Meanwhile, multiple pathways of tumor cell-induced platelet activation (TCIPA) have been identified.[19,20] LMWH was shown to interfere with TCIPA to prevent the formation of cancer cell/platelet heteroaggregates and platelet degranulation.[21,22]

However, from a chemical point of view, heparin is a nonideal drug representing a linear highly sulfated polysaccharide. Heparin is of natural origin and thus has underlying variations in saccharide composition and size. The main problematic issue referring to heparin is related to its isolation from animal sources. Besides the potential risk of contamination, its production may run into serious limitations in the supply chain.[23] In light of the clinically established role of heparins as anticoagulants for decades, the structural variations in the heparin molecule are considered as a well-balanced issue for targeted activities. The chemical peculiarities of a sulfated natural polymer were discussed in terms of pleiotropic activities, especially in the context of cancer. Nevertheless, heparin and LMWH can cause major adverse events, for example, heparin-induced thrombocytopenia, and also possess therapeutic limitations, such as a narrow therapeutic window and variations in bioavailability and pharmacokinetics.[24,25] However, there is a growing interest in synthetic approaches to generate polymeric heparin mimics that can provide a better control over structure, sulfation, molecular size dispersity, and purity. Several chemical structures as potential heparin mimetics have been introduced into different stages of preclinical tests.[26−28] Recently, we have introduced a series of noncarbohydrate heparin mimetics produced by the reversible addition−fragmentation chain transfer (RAFT) polymerization of sulfonated and carboxylated monomers. Homopolymers, ranging in size from 5 to 50 kDa, were prepared from sodium 4-styrenesulfonate (SSS), sodium-2-acrylamido-2-methyl-1-propane sulfonate (AMPS), potassium-3-sulfopropyl acrylate (SPA), and potassium-3-sulfopropyl methacrylate (SPM).[29] Furthermore, copolymers of these sulfonated monomers were also prepared and investigated with respect to their anticoagulant activities.[30] Notably, the homopolymers displayed different levels of anticoagulant activity, dependent on the MW and monomer composition, with poly(SSS) emerging as the most potent. Copolymers consisting of sulfonated monomers and acrylic acid (AA) were also promising anticoagulants, with copolymers of SSS and AA also featuring anti-FIIa activity, and all inducing prolonged activated partial thromboplastin time (APTT) and thrombin clotting time (TCT).[29] However, the potential activity of these heparin mimics for oncological applications remains to be explored.

Here, we aimed to investigate whether the potential antithrombotic activity of the polymers is sufficient to interfere with molecular mechanisms simulating the metastatic spread of tumors in vitro, namely, different aspects of TCIPA. To further consider other probably coagulation-independent heparin targets of metastasis, we also focused on cell adhesion receptors by biosensor and microscopic approaches. Here, we demonstrate that platelet activation is strongly attenuated by the anticoagulant polymers poly(SSS), and more promising poly(SSS-*co*-AA) of different MWs, represented by platelet aggregation and platelet degranulation approaches. Furthermore, these promising candidates display an impressive

https://doi.org/10.1021/acsami.0c20744
ACS Appl. Mater. Interfaces 2021, 13, 7080−7093

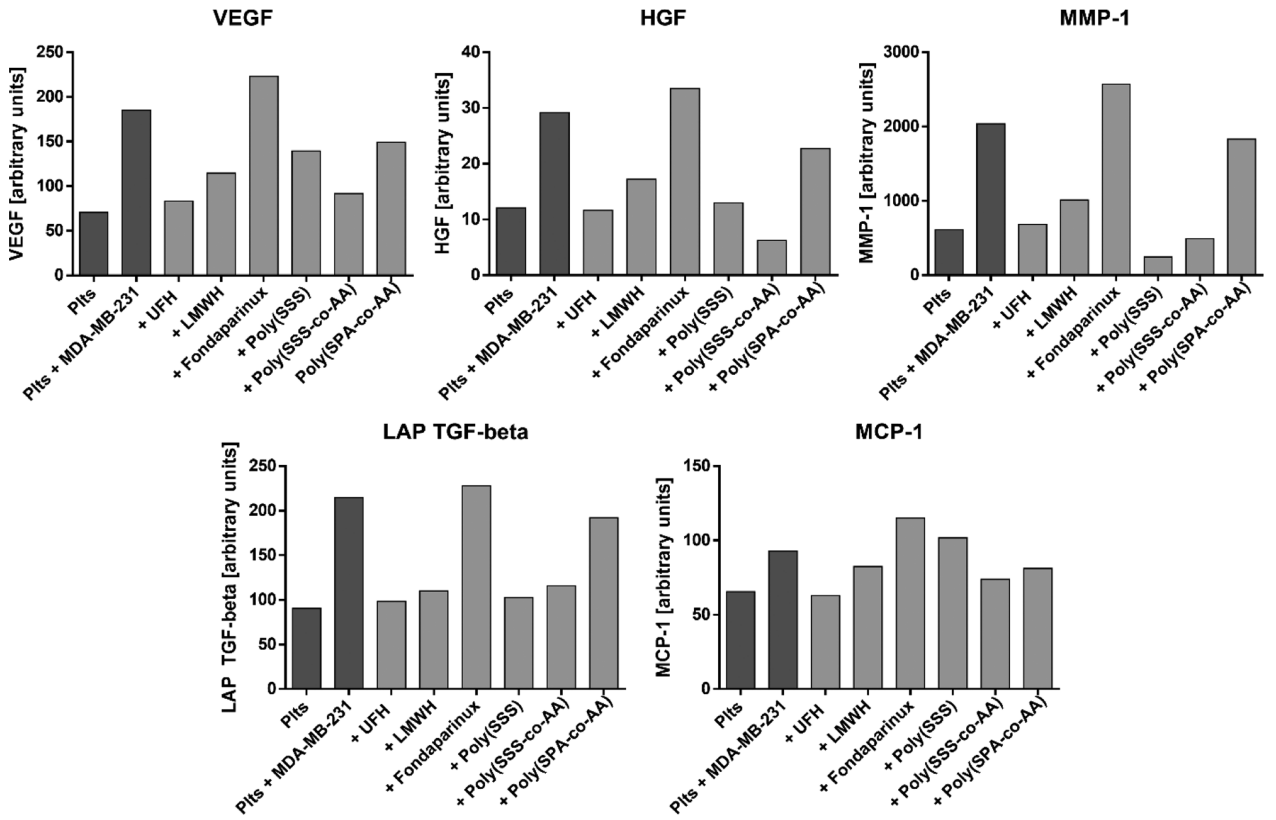

Figure 2. Poly(SSS) and poly(SSS-*co*-AA) heparin mimetics strongly attenuate tumor cell-induced platelet degranulation. Release of proteins from platelet granules after stimulation with MDA-MB-231 breast cancer cells. Relative protein levels were determined by Olink Bioscience Inflammation panel after preincubation with the indicated compounds at 50 μg/mL and adopted therapeutic concentrations, respectively. The three polymers were applied at a molecular mass of 20 kDa and a monomer ratio of 1:1. $N = 1$.

capacity to block the enzymatic activity of heparanase and the adhesive functions of P-selectin and the integrin VLA-4 in a coagulation-independent manner, outmatching heparin and LMWH. These data emphasize these noncarbohydrate copolymers as promising novel chemical candidates for therapeutic antimetastatic approaches. Finally, these molecules may help us to answer yet open questions on the beneficial role of heparins in oncology due to their highly defined, heparin-mimicking structures.

RESULTS

Heparin-Mimicking Polymers Impair Tumor Cell-Induced Platelet Aggregation. Platelets are the first host cell population that tumor cells encounter after arrival in the blood circulation. The immediate contact between tumor cells and platelets, forming a platelet cloak around the tumors, induces platelet activation. Heparin was shown to prevent this activation by anticoagulant and antiadhesive activities.[31] The recently introduced synthetic heparin mimetics display pronounced anticoagulant activities.[29] However, it remains open whether they are also able to interfere with TCIPA similarly to heparin. To elucidate this, we first selected platelet aggregation as a recognized screening system for TCIPA. Therefore, we applied five different homopolymers, namely, poly(SSS), poly(AMPS), poly(SPA), poly(SPM), and poly(AA) at a selected, heparin-related molecular weight of 20 kDa and screened for their capacity to abrogate cancer cell-induced platelet aggregation in light transmission aggregometry (LTA) (Table 1, Figure 1). Furthermore, we also included some selected copolymers at this indicated molecular weight for this approach, all the polymers display low dispersities with $Đ$ between 1.08 and 1.38, as described before (Table S1).[29,30] The platelets were preincubated with 50 μg/mL polymer to compare their inhibitory capacities on a weight basis, before MDA-MB-231 human breast cancer cells were added to induce aggregation. The copolymer poly(SSS-*co*-AA) exhibited the strongest inhibition of platelet aggregation. Four other polymers containing the SSS monomer were also revealed as potent inhibitors of platelet aggregation. In contrast, polymers lacking the SSS monomer in their composition failed to affect cancer cell-mediated platelet aggregation. Thus, the SSS monomer seems to be the crucial building block for an inhibitory activity.

Based on the results of this first LTA screening, poly(SSS) and poly(SSS-*co*-AA) compounds were considered as the most promising candidates for further investigations concerning the capacity of these heparin-mimicking polymers to interfere with the cancer cell−platelet interaction. To investigate whether and how the molecular weight of the indicated compounds poly(SSS) and poly(SSS-*co*-AA) affects their inhibitory capacities on MDA-MB-231 breast cancer cell-induced aggregation, we selected poly(SSS) and the copolymer poly(SSS-*co*-AA) at varying sizes of 5, 10, 20, and 50 kDa in the LTA assay, choosing again a 50 μg/mL concentration of the compounds (Figure 1). For a better evaluation of the data, commercial anticoagulants such as unfractionated heparin (UFH), the LMWH enoxaparin, and the pentasaccharide fondaparinux were applied at adopted therapeutic concentrations. The thrombin receptor activator TRAP-6 was

https://doi.org/10.1021/acsami.0c20744
ACS Appl. Mater. Interfaces 2021, 13, 7080−7093

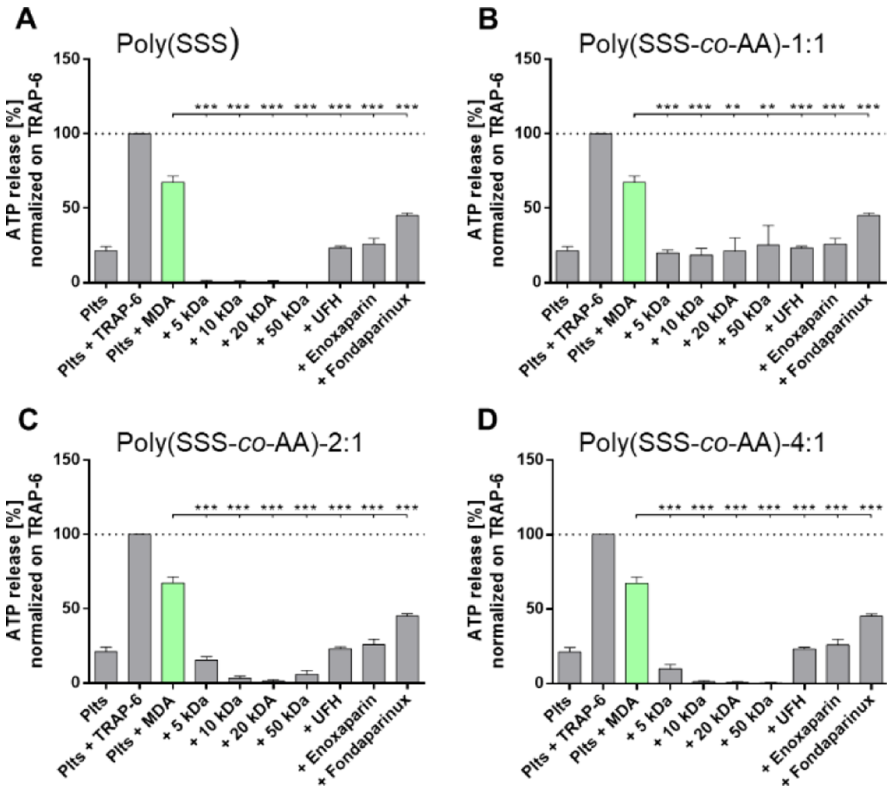

Figure 3. Inhibition of tumor cell-induced dense granule release by heparin-mimicking polymers. Platelets were preincubated with (A) poly(SSS), (B) poly(SSS-*co*-AA)-1:1, (C) poly(SSS-*co*-AA)-2:1, and (D) poly(SSS-*co*-AA)-4:1 at varying molecular weights. Polymers were applied at 50 μg/mL while the commercial heparin derivatives referred to therapeutic concentrations. After stimulation with MDA-MB-231 breast cancer cells, platelet ATP release was determined by a luciferase-based assay. Data are represented as mean ± SD. *: $p < 0.05$; **: $p < 0.01$; and ***: $p < 0.001$.

considered as a positive control to induce maximal platelet aggregation.

Notably, reducing the molecular weight from 20 to 10 or 5 kDa, respectively, did not affect the high potential of both poly(SSS) and the copolymers to block cancer cell-induced platelet aggregation (Figure 1A–D). The indicated heparin mimetics are as efficient as UFH and enoxaparin (Figure 1E). However, the polymers at the highest MW of 50 kDa displayed some divergent effects and appeared less efficient in inhibition of platelet aggregation. The 50 kDa poly(SSS) may induce platelet aggregation itself as platelets started to aggregate at the beginning of the measurement and even before aggregation was induced by the addition of MDA-MB-231 cells (Figure 1A). However, we cannot fully explain this size effect presently, but the excellent inhibitory capacities of the poly(SSS-*co*-AA) derivatives at the lower MW are remarkable and warrant further investigations. Concerning the molecular basis of these effects, since the Xa inhibitor fondaparinux failed to induce inhibition in this assay, the activity of the polymers and the indicated heparins appears to be, at least in part, related to a combined antiadhesive and anticoagulant activity. This appears in line with others studies on anticoagulant polymeric heparin mimetics that failed to show an anti-Xa activity.

Poly(SSS) and Poly(SSS-*co*-AA) Heparin Mimetics Strongly Attenuate Tumor Cell-Induced Platelet Degranulation. Besides the direct aggregate formation between cancer cells and platelets, the content of platelet granules crucially contributes to cancer cell survival and metastasis. To achieve initial insights into the inhibitory capacities of the heparin-mimicking polymers to affect granule release, we chose the most promising compounds from the LTA screening, poly(SSS-*co*-AA)-1:1 20 kDa copolymer, as well as the poly(SSS) 20 kDa polymer, and as a negative control, the noninhibiting poly(SPA-*co*-AA)-1:1 20 kDa compound. For comparison, protein release from platelet α-granules after treatment with the commercial heparins was examined (Figure 2). Several proteins stored in platelets' α-granules are described to be involved in metastatic spread.[32] Hence, we used the proximity extension assay (PEA) by Olink Bioscience to determine levels of a variety of proteins occurring in the secretome upon platelet activation. As expected, the activation with MDA-MB-231 cells led to an increased release of VEGF, HGF, MMP-1, LAP TGF-beta, and MCP-1 compared to quiescent platelets. In accordance with the LTA screening data mentioned above, UFH demonstrated the best inhibitory capacities among the commercially available heparins, while fondaparinux had no effect to attenuate the protein release. Again, poly(SSS-*co*-AA)-1:1 20 kDa copolymer and the poly(SSS) 20 kDa kept up with UFH and showed remarkable inhibition of platelets' granule release. Notably, poly(SPA-*co*-AA)-1:1 20 kDa that was expected to be inefficient based on the aggregation data in Table 1 indeed showed hardly any inhibitory capacities.

To evaluate whether the indicated polymers affect platelet degranulation more comprehensively beyond α-granule release, we next applied a detailed quantification of ATP release as a representative constituent of platelets' dense granules. Therefore, the ATP release after platelet activation by MDA-MB-231 cells was quantified by a luminescence measurement. The capacity of the heparin mimetic polymers and the impact of their size and compositions on platelet ATP release were compared to the activity of commercial heparins.

https://doi.org/10.1021/acsami.0c20744
ACS Appl. Mater. Interfaces 2021, 13, 7080–7093

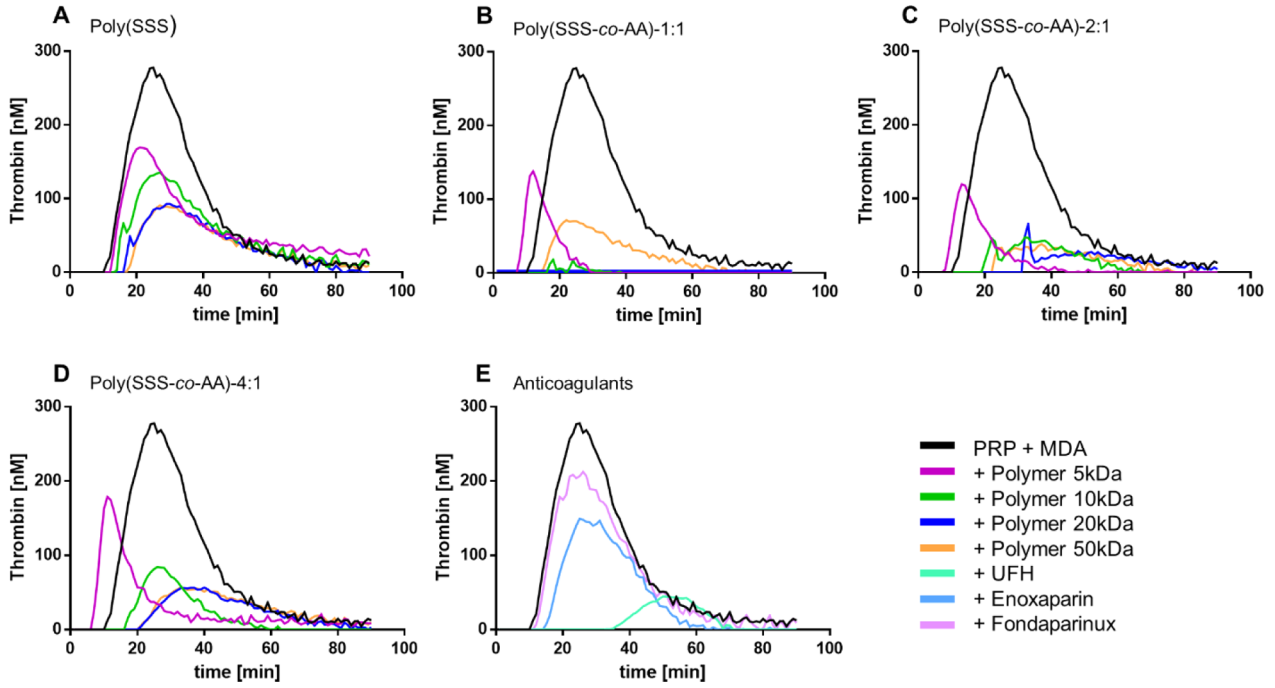

Figure 4. Indicated heparin mimetics inhibit cancer cell-induced coagulation. PRP was incubated with varying sizes of (A) poly(SSS), (B) poly(SSS-*co*-AA)-1:1, (C) poly(SSS-*co*-AA)-2:1, and (D) poly(SSS-*co*-AA)-4:1 at a concentration of 600 μg/mL. Thrombin generation was induced by MDA-MB-231 cells and monitored for 90 min. (E) Comparative values of UFH (1 IU/mL), enoxaparin (1 IU/mL), and fondaparinux (775 ng/mL) were recorded. Representative graphs of thrombin generation kinetics are shown. See also Figures S2 and S3.

Untreated platelets or platelets activated by TRAP-6 were considered as negative or positive controls, respectively. Regarding the poly(SSS) polymer (Figure 3A) and the poly(SSS-*co*-AA) 2:1 and 4:1 copolymers (Figure 3C,D), it seems that SSS or higher proportions of SSS might cause some unknown interference in the detection of ATP since the ATP levels were partially reduced below the levels of nonactivated platelet controls. In contrast, in the case of the copolymer poly(SSS-*co*-AA)-1:1 (Figure 3B), ATP release is attenuated to the level of nonactivated platelet control. Although we cannot totally exclude the indicated unspecific interference also in this case, the luminescence data refer to an impressive capacity to attenuate ATP release by this copolymer, at least as active as, or partly exceeding the activities of UFH and enoxaparin. Again, fondaparinux is less potent in this experimental approach to block platelet activation and dense granule release. However, these data further confirm the capacities of the indicated polymers to abrogate platelet activation by cancer cells.

Indicated Heparin Mimetics Inhibit Cancer Cell-Induced Coagulation. TCIPA is often covered or initiated by the activation of the plasmatic coagulation cascade and generation of thrombin. For this, tissue factor expressed by tumor cells acts as an initial stimulus for local thrombin formation. Thrombin, in turn, activates human platelets by cleavage of PAR-1, PAR-4, and GPIbα, respectively, and additionally exerts multiple prometastatic effects.[33] MDA-MB-231 cells express tissue factor, so their impact on TCIPA via the thrombin pathway is highly relevant for the platelet aggregation shown above.[21] Notably, our recent data referred to the fact that tumor cell-induced thrombin formation appeared complex and more challenging for inhibitory approaches than thrombin formation by recombinant tissue factor.[21] In recent studies, poly(SSS) and the poly(SSS-*co*-AA) exhibit strong inhibitory effects on tissue factor-induced thrombin formation.[29] Thus, it remains questionable whether the heparin mimetics are also able to interfere with tumor cell-induced thrombin formation. Therefore, platelet-rich plasma (PRP) was incubated with the different compounds, and the kinetics of thrombin formation after activation with MDA-MB-231 cells were recorded (Figure 4). Polymers consisting solely of the SSS building block were less efficient in blocking cancer cell-induced thrombin generation. Interestingly, the blocking capacity increased with the molecular size of the SSS polymer (Figure 4A). Nevertheless, in general, they showed anticoagulant activities, which appeared comparable to the LMWH enoxaparin (Figure 4E). Variation of the monomer ratio in poly(SSS-*co*-AA) copolymers (Figure 4B–D) led to a more versatile inhibition pattern.

In general, the lowest molecular weight of 5 kDa appeared less favorable for the anticoagulant effects in all three copolymers. They show the weakest inhibitory capacities and, interestingly, seem to support fast thrombin generation, resulting in an earlier onset of thrombin formation compared to the positive control of MDA-MB-231-activated PRP. In contrast, the higher-molecular-weight copolymers displayed an impressive activity, which partly exceeds the effects of UFH. Decreasing the SSS proportion in the compounds, there was a switch between 10 and 50 kDa resulting in stronger inhibition of thrombin formation by the 10 kDa polymer for the poly(SSS-*co*-AA)-1:1 compound. However, the 20 kDa copolymers exhibit the strongest inhibition of thrombin formation among the variations of molecular size, which was equal or even better than UFH in the case of poly(SSS-*co*-AA)-1:1.

Poly(SSS) and Poly(SSS-*co*-AA) Mimetics Strongly Bind to P-Selectin and VLA-4 and Attenuate Tumor Cell Binding. The antimetastatic capacities of heparin or

https://doi.org/10.1021/acsami.0c20744
ACS Appl. Mater. Interfaces 2021, 13, 7080−7093

Table 2. P-Selectin-Binding Kinetics of UFH, the LMWH Enoxaparin, and the Pentasaccharide Fondaparinux Compared to the Heparin-Mimicking Polymers[a]

compound	K_D [M]	k_{on} [M^{-1} s^{-1}]	k_{off} [s^{-1}]
UFH	$2.35 \times 10^{-8} \pm 0.39 \times 10^{-8}$	$3.15 \times 10^{5} \pm 0.42 \times 10^{5}$	$7.64 \times 10^{-3} \pm 2.20 \times 10^{-3}$
enoxaparin	$2.27 \times 10^{-7} \pm 0.32 \times 10^{-7}$	$9.97 \times 10^{4} \pm 2.04 \times 10^{4}$	$1.86 \times 10^{-2} \pm 0.21 \times 10^{-2}$
fondaparinux	n.d.	n.d.	n.d.
poly(SSS) 20 kDa	$2.50 \times 10^{-7} \pm 0.17 \times 10^{-7}$	$4.56 \times 10^{4} \pm 0.55 \times 10^{4}$	$8.30 \times 10^{-3} \pm 3.60 \times 10^{-3}$
poly(SSS-*co*-AA)-1:1 10 kDa	$3.86 \times 10^{-7} \pm 1.69 \times 10^{-7}$	$5.08 \times 10^{4} \pm 1.49 \times 10^{4}$	$1.80 \times 10^{-2} \pm 0.48 \times 10^{-2}$
poly(SSS-*co*-AA)-1:1 20 kDa	$2.19 \times 10^{-7} \pm 0.51 \times 10^{-7}$	$6.27 \times 10^{4} \pm 0.61 \times 10^{4}$	$1.33 \times 10^{-2} \pm 0.19 \times 10^{-2}$
poly(SPA-*co*-AA)-1:1 20 kDa	$5.70 \times 10^{-7} \pm 1.77 \times 10^{-7}$	$5.34 \times 10^{4} \pm 2.19 \times 10^{4}$	$2.95 \times 10^{-2} \pm 1.02 \times 10^{-2}$

[a]Data represent mean (n = 3) ± SD.

Table 3. VLA-4-Binding Kinetics of UFH, the LMWH Enoxaparin, and the Pentasaccharide Fondaparinux Compared to the Heparin-Mimicking Polymers[a]

compound	K_D [M]	k_{on} [M^{-1} s^{-1}]	k_{off} [s^{-1}]
UFH	$1.09 \times 10^{-6} \pm 0.24 \times 10^{-6}$	$3.41 \times 10^{4} \pm 1.15 \times 10^{4}$	$3.21 \times 10^{-2} \pm 1.18 \times 10^{-2}$
enoxaparin	n.d.	n.d.	n.d.
fondaparinux	n.d.	n.d.	n.d.
poly(SSS) 20 kDa	$1.63 \times 10^{-7} \pm 0.09 \times 10^{-7}$	$7.82 \times 10^{4} \pm 0.19 \times 10^{4}$	$1.25 \times 10^{-2} \pm 0.11 \times 10^{-2}$
poly(SSS-*co*-AA)-1:1 10 kDa	$4.07 \times 10^{-7} \pm 0.48 \times 10^{-7}$	$6.73 \times 10^{4} \pm 0.71 \times 10^{4}$	$2.47 \times 10^{-2} \pm 0.19 \times 10^{-2}$
poly(SSS-*co*-AA)-1:1 20 kDa	$3.43 \times 10^{-7} \pm 1.08 \times 10^{-7}$	$5.94 \times 10^{4} \pm 1.56 \times 10^{4}$	$1.78 \times 10^{-2} \pm 0.13 \times 10^{-2}$
poly(SPA-*co*-AA)-1:1 20 kDa	n.d.	n.d.	n.d.

[a]Data represent mean (n = 3) ± SD.

LMWH are based on multiple molecular modes of action, and besides the anticoagulant, and thus antiplatelet activating properties, antiadhesive capacities have been regarded as crucial contributions. P-selectin, expressed on both platelets and endothelial cells, has been considered as a primary target of heparin, attenuating the contact formation with platelets and vascular surface and thus interfering with the metastatic process of tumor cells.[34] The binding kinetics of heparin and LMWH to P-selectin have been investigated by different approaches.[35,36] To investigate whether the heparin mimetics poly(SSS) and selected copolymers have also a binding affinity to P-selectin, we performed a surface acoustic wave (SAW) biosensor approach. Therefore, recombinant P-selectin was inserted into a sensor-fixed model membrane in a his-tag-orientated manner and binding of heparin or the polymers to immobilized P-selectin was analyzed under dynamic flow conditions. Besides the most promising compounds poly(SSS-*co*-AA)-1:1, 10 kDa and 20 kDa, identified in the assays mentioned above, or poly(SSS) 20 kDa, the poly(SPA-*co*-AA)-1:1 20 kDa was applied as a control to evaluate whether simply a negative charge density of the compound is sufficient or the 4-styrenesulfonate structure is superior in terms of P-selectin binding. As indicated in Table 2, UFH possesses the highest P-selectin affinity in the mean nanomolar range. The LMWH enoxaparin displayed a bit lower affinity in the high nanomolar range, while P-selectin binding of the pentasaccharide fondaparinux was not detectable. Notably, both poly(SSS) and poly(SSS-*co*-AA) 20 kDa have similar affinities to enoxaparin, while the 10 kDa copolymer has a slightly reduced affinity. Surprisingly, although the poly(SPA-*co*-AA) 1:1 copolymer failed to show activity in the coagulation-dependent assay mentioned above, it displayed a remarkable affinity to P-selectin.

The integrin VLA-4 is also blocked by heparin in its binding capacities to the ligand VCAM-1 with strong consequences to attenuate the metastasis of melanoma cells expressing VLA-4.[37] Although some initial structure−activity relationships have been derived for heparin binding to VLA-4, the binding of the heparin mimetics to VLA-4 is completely ambiguous and appears as another attractive target in potential antimetastatic approaches. To follow this, we again applied the SAW biosensor approach, using recombinant, his-tagged VLA-4 inserted into the sensor-fixed model membrane. As shown in Table 3, UFH was the only commercial heparin, which displays a remarkable binding toward the integrin VLA-4. Neither enoxaparin nor fondaparinux were able to bind VLA-4, which makes a certain molecular size dependency a likely decisive factor for the VLA-4-binding capacity.

As shown in Table 3, the three SSS-containing compounds outrange the binding affinity of UFH, whereas there was no VLA-4 binding detectable for the poly(SPA-*co*-AA)-1:1 lacking the 4-styrenesulfonate. Regarding the molecular composition of 20 kDa-sized molecules, a polymer of pure SSS monomers seems more favorable than the copolymer of SSS and AA, represented by the K_D values of 1.63×10^{-7} and 3.43×10^{-7} M, respectively. By scaling the molecular size of the copolymer down to 10 kDa, the binding affinity was further reduced to a K_D value of 4.07×10^{-7} M. Again, this refers to the fact that a certain molecular size is obviously required for VLA-4 binding.

To characterize the functional consequences of VLA-4 cell binding, a flow chamber assay was established to evaluate the capacities of the heparin mimetics to inhibit the VLA-4-mediated cell binding. Therefore, binding of VLA-4 expressing MV3 melanoma cells to the immobilized ligand VCAM-1 was assessed microscopically under physiological shear stress, and the impact of heparin and heparin mimetics thereon was quantified. First, MV3 wt cells were investigated for their binding toward VCAM-1, either in a VLA-4 inactive or an activated VLA-4 state by adding Mn^{2+}. As shown in Figure 5A, activated MV3 wt cells adhere strongly to the VCAM-1-covered glass slides, while only 20% of nonactivated cells were bound to immobilized VCAM-1. To explore the influence of unspecific cell binding and further focus on the impact of VLA-4 on binding, we applied an MV3-β1-integrin knockdown

https://doi.org/10.1021/acsami.0c20744
ACS Appl. Mater. Interfaces 2021, 13, 7080−7093

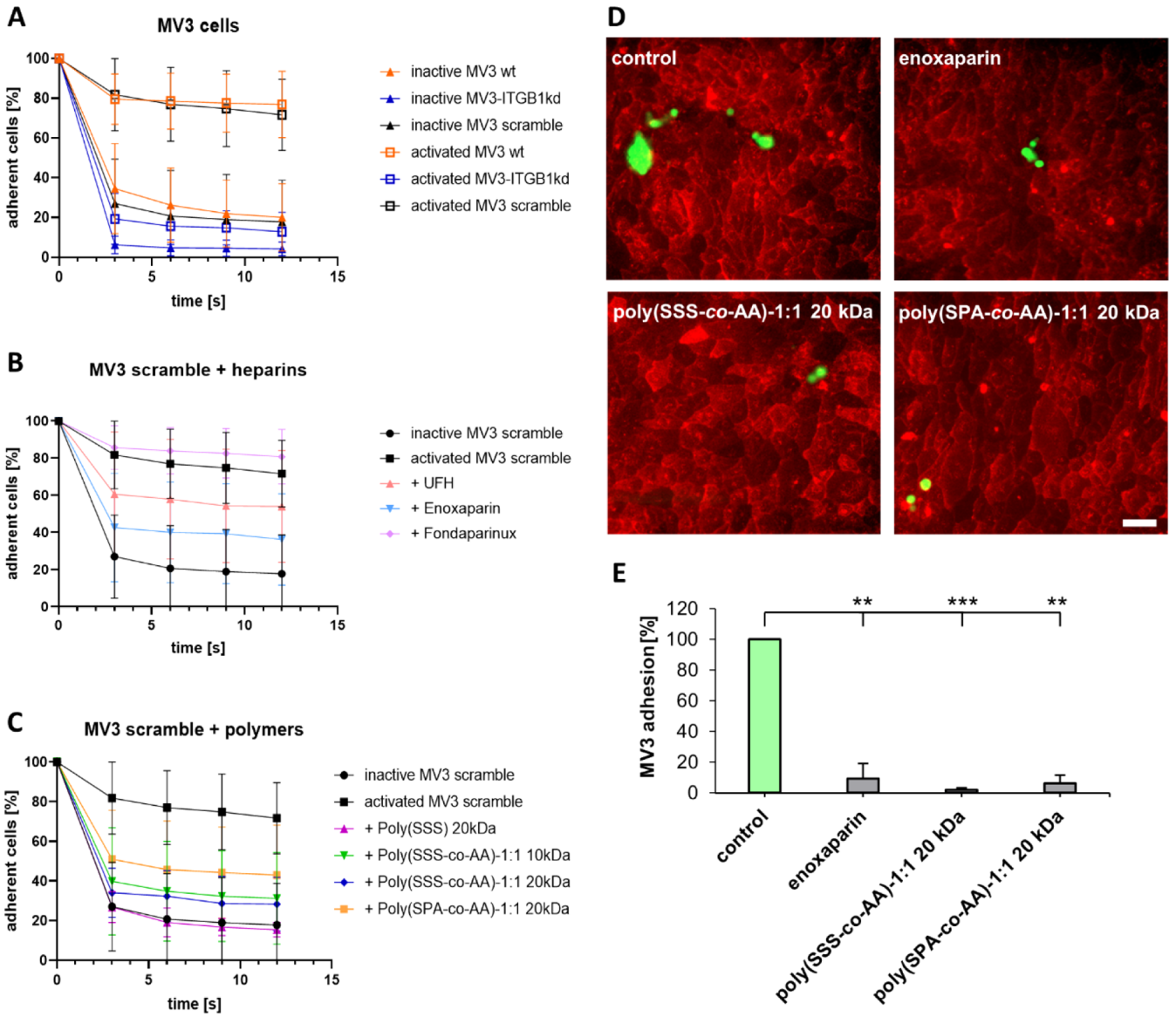

Figure 5. Indicated heparin mimetics block VLA-4-mediated cell binding and inhibit MV3 cell binding to artificial blood vessels with impressive capacity. (A) MV3 wt cells, MV3-ITGB1kd cells, and scramble kd cells were incubated with 1 mM Mn^{2+} to activate VLA-4 (activated) or were left nonactivated for binding toward immobilized VCAM-1. MV3 wt and MV3 scramble strongly bind upon activation, while MV3-ITGB1kd did not respond to activation and remained at the binding level of the nonactivated cells. (B) MV3 scramble cells were incubated with adopted therapeutic concentrations of UFH, enoxaparin, and fondaparinux to interfere with activated VLA-4. (C) MV3 scramble cells were incubated with 50 μg/mL of the indicated heparin-mimicking polymers during the Mn^{2+} activation. (D,E) HUVECs were continuously perfused with whole hirudin blood spiked with 1×10^6 MV3 cells for 30 min. (D) Representative images of MV3 cells (green) attached to the HUVEC layer (red) are shown. Scale bar = 100 μm. Prior to the perfusion, MV3 cells were either treated only with 1 mM $MnCl_2$ (control) or additionally with enoxaparin (1 I.E/mL), poly(SSS-*co*-AA)-1:1 20 kDa (50 μg/mL), or poly(SPA-*co*-AA)-1:1 20 kDa (50 μg/mL). (E) MV3 adhesion was analyzed in more than 500 fields of view of 3−4 independent experiments. Data are represented as mean ± SD. *: $p < 0.05$; **: $p < 0.01$; and ***: $p < 0.001$.

(MV3-ITGB1kd) variant and its corresponding scramble control (Figure 5A). MV3-ITGB1kd cells showed barely any adhesion upon activation by Mn^{2+} indicating only a very small influence of unspecific binding events. The scramble control showed similar adherence compared to the MV3 wt cells in Figure 5A and were used in the further investigations.

In accordance with the prior VLA-4-binding study, UFH reduced the adhesion of the activated cells, whereas fondaparinux did not reduce cell binding to VCAM-1. Enoxaparin, for which no VLA-4 binding affinity was detected, diminished the adherence of MV3 scramble cells under physiological flow conditions below the level of UFH (Figure 5B). Notably, the investigated polymers confirmed their VLA-4 binding by reducing the adhesion of the activated scramble control clearly, with the polymer poly(SSS) 20 kDa showing the strongest inhibitory capacity down to the basal level of inactivated MV3 scramble cells, which is comparable to an ITGB1 knockdown. Surprisingly, poly(SPA-*co*-AA)-1:1 20 kDa, the compound which displayed no detectable VLA-4 binding, was also effective in blocking the VLA-4/VCAM-1-mediated cell binding and kept up close to the inhibitory capacities of both poly(SSS-*co*-AA) (Figure 5C).

To further adapt to physiological tumor cell-binding conditions, we applied an artificial blood vessel assay, in

https://doi.org/10.1021/acsami.0c20744
ACS Appl. Mater. Interfaces 2021, 13, 7080−7093

which MV3 melanoma cells binding to endothelial cells can be visualized in a simulated venous blood flow in full blood. Thus, P-selectin and VLA-4 act in synergy and can be investigated with respect to the inhibitory capacity of heparin or heparin mimetics simultaneously. As indicated in Figure 5D,E, the adhesion of MV3 cells to endothelial cells was strongly inhibited by poly(SSS-*co*-AA)-1:1 20 kDa which confirms its high capacity to block P-selectin and VLA-4 binding. Both, the LMWH enoxaparin and the non-anticoagulant poly(SPA-*co*-AA)-1:1 20 kDa demonstrated binding inhibition to a similar extent, even though they did not bind to VLA-4 in the SAW biosensor approach. However, these findings support the observation that enoxaparin and poly(SPA-*co*-AA)-1:1 20 kDa are capable to block, beside P-selectin, VLA-4-mediated interactions.

The heparin mimetics did not display any toxic effects to EA.hy926 endothelial cells, as indicated in supplementary Figure 4.

Poly(SSS-*co*-AA) is an Excellent Inhibitor of Heparanase Activity. Heparanase is an endoglycosidase and the sole enzyme in mammalian organisms able to cleave heparan sulfate (HS) chains. Heparanase is considered as a marker for bad prognosis indicating growth, angiogenetic activity, and metastatic spread of tumors. Based on the structural similarities of heparin and HS, heparin has been used as an inhibitor of heparanase and as a scaffold to derive more potent antagonists. Blocking heparanase is recognized as a primary mode of action when discussing potential antitumor effects of heparin in oncology. In order to evaluate whether the indicated heparin mimetics also possess inhibitory potencies against heparanase, we applied a fluorescence-based activity assay. As indicated, poly(SSS) 20 kDa and the two copolymers poly(SSS-*co*-AA)-1:1 with 10 and 20 kDa displayed impressive high inhibitory capacities, showing the best results for the 20 kDa compound (Figure 6). Notably, poly(SPA-*co*-AA) is in a similar activity range. Compared to the LMWH enoxaparin, which displayed an IC_{50} of 367.6 nM, the heparin-mimicking polymers revealed a roughly tenfold higher capacity to inhibit heparanase. Impressively, the clinical candidate for heparanase inhibition PG545, which is indeed better than LMWH (IC_{50} 187.3 nM), was also outmatched by the heparin mimetics indicating a remarkable potency of the indicated polymers to block heparanase.

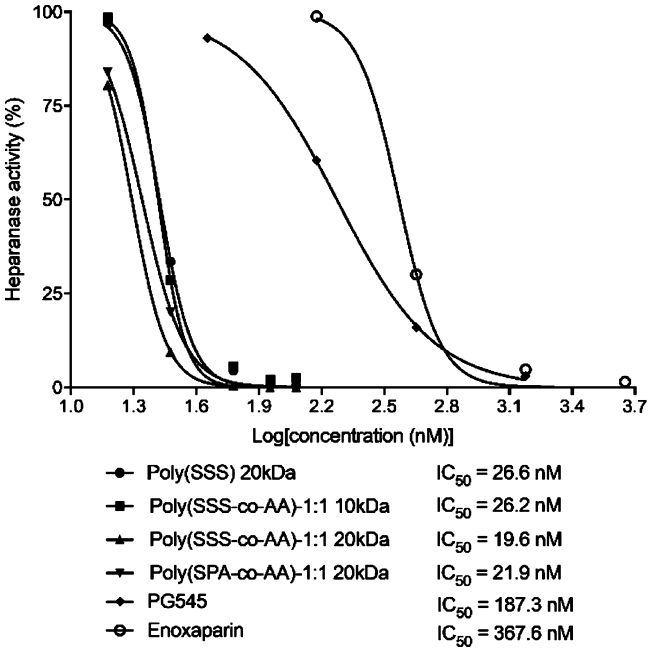

Figure 6. Compounds at the concentrations indicated were incubated with semipurified heparanase first and then the substrate was added. After incubation at 37 °C for 30 min, the heparanase activity was detected by reading HTRF signals (ratio between 665 and 620) and expressed as a percentage of heparanase activity. The data refer to an impressive inhibitory capacity of the mimetics to inhibit heparanase, outperforming the LMWH enoxaparin by roughly tenfold higher activity and even exceeding the clinical candidate PG545. Data are represented as mean from two independent experiments. Data of enoxaparin are presented as mean from one experiment. Each experiment was run in triplicate.

DISCUSSION

Promise of Heparin Mimetics as Anticoagulants. Despite the clinical acceptance of LMWH in oncological treatment, the question whether heparinization of cancer patients has additional antitumoral benefits beyond anticoagulation is not fully answered yet. This is mainly related to structural issues of heparin since structural heterogeneities complicate the search for further targets, which probably contribute to a potential survival benefit. Nevertheless, structural requirements for antithrombotic activities within heparin's natural heterogeneities have been elucidated defining the imperative of the pentasaccharide antithrombin binding unit and a critical degree and position of sulfation of the GAG backbone. Although several approaches exist to differentiate antithrombotic and other activities in preclinical oncological approaches, the resulting non-antithrombotic heparin derivatives still suffer from the non-well-defined structural peculiarities of the heparin scaffold.[38]

In these terms, synthetic polymers mimicking the heparin structure could be a helpful tool. Several studies focused on the generation of synthetic heparin mimetics as potential anticoagulants, which promises a controlled tuning of binding parameters, a higher stability of the polymers compared to heparin, and an easier functionalization to obtain derivatives for structure−activity relationships.[26,27] All these peculiarities of synthetic mimetics were discussed to potentially overcome therapeutic drawbacks of heparin and LMWH; however, a clinical reflection of those promises is still open. Nevertheless, those considerations do not exist for oncological applications, which are for the first time described here.

We have recently introduced a series of nontoxic sulfonated polymers, prepared by RAFT polymerization. These polymers and copolymers displayed, depending on the MW, increased TCT and APTT, two thrombin-related clinical parameters reflecting certain antithrombotic activities. However, none of the polymer mimetics displayed anti-FXa activity.[29] Here, we investigated members of this series in an oncological context characterizing their inhibitory activities in different steps of the simulated metastatic spread, not only in anti-thrombotically related assays of TCIPA but also in non-antithrombotically driven approaches.

Heparin Mimetics as an Antimetastatic Approach—Structural Consideration of Antithrombotic-Related Activities. We highlight poly(SSS) and the copolymers poly(SSS-*co*-AA) as an anticoagulant and most active mimetics affecting platelet activity, from which poly(SSS-*co*-AA)-1:1 at a 10 or 20 kDa MW appear as the outstanding candidates

https://doi.org/10.1021/acsami.0c20744
ACS Appl. Mater. Interfaces 2021, 13, 7080−7093

throughout all assays. From a structural point of view, all polymers of the series differ in the backbone structure but more importantly in the side chain flexibility, conformation, and thus presentation of the sulfonate negative charge. Our data clearly indicate that the presence of styrenesulfonate appears as a critical component to obtain any antithrombotic activity. On the basis of the general requirement of styrenesulfonate, a certain impact of charge/sulfonate density appears likely taking the 1:1 ratio of SSS/AA as optimum in the (SSS-*co*-AA) copolymers, while higher sulfonate densities with increasing SSS/AA ratio attenuated the activities or in the case of poly(SSS) give rise to unspecific, may be charge-induced side effects. However, the presentation of sulfonate as either a sodium or potassium salt appears not decisive. Concerning the impact of MW on the activity of poly(SSS) or more likely the poly(SSS-*co*-AA), derivatives of UFH comparable to MW of 10 or 20 kDa were most active, while the longer 50 kDa compounds tend to display unwanted effects, as shown for intrinsically induced platelet aggregation. However, our data confirm that the poly(SSS) and poly(SSS-*co*-AA) at the mean MW are highly potent to inhibit cancer cell-induced platelet aggregation and granule secretion, two key processes contributing to the tumor cell protection and metastatic niche formation in the course of hematogenous metastasis. The indicated mimetics were as competent or even better than LMWH. Data of the thrombin formation assays confirm that attenuated platelet activation was mainly driven by the antithrombotic activities of the indicated mimetics. Furthermore, anti-FXa activity, represented by the pentasaccharide fondaparinux, is obviously not sufficient in these terms and did not contribute to the activity spectrum of the heparin mimetics.

Heparin Mimetics as Antimetastatic Agents—Non-antithrombotic-Related Mode of Action. In light of these findings, it is noteworthy that the poly(SSS-*co*-AA) copolymers also exceed other compounds, including LMWH, in three thrombin-independent assays, namely, the binding of P-selectin, integrin VLA-4, and heparanase inhibition. Interestingly, the differences within the polymers appears less-pronounced since poly(SPA-*co*-AA)-1:1 copolymer, indicated as a negative control in the thrombin-related assays mentioned above, displays a remarkable activity in the assays ranging only slightly behind the poly(SSS-*co*-AA) copolymer. Heparanase and the adhesion receptors P-selectin and VLA-4 are key players in the metastatic cascade, and their attenuation by heparin is regarded as an important mode of action. The role of P-selectin as a target for heparin in attenuating metastatic spread was intensively investigated, and structural requirements of heparin and non-anticoagulant heparin derivatives are known to block P-selectin binding.[34] Notably, in terms of these tight structural necessities for heparin to inhibit P-selectin, that is, position of sulfation, the high capacities of the mimetics to bind to and block P-selectin are an interesting finding. Concerning VLA-4, the integrin is known as an adhesion receptor in melanoma metastasis and associated with macrophage recruitment to circulate tumor emboli.[39] The combined activity of the mimetics, that is, poly(SSS-*co*-AA) to bind and block both, P-selectin and VLA-4, was confirmed in the artificial blood vessel assay on MV3 cell binding to endothelium, outmatching the activity of the LMWH enoxaparin.

Heparanase is considered as a marker for bad prognosis indicating growth, angiogenetic activity, and metastatic spread of tumors.[40] Degradation of HS structures by heparanase has important implications for remodeling of the cellular microenvironment and thus has direct impact on growth, extravasation, and metastasis of cancer.[41] The activity of poly(SSS-*co*-AA) copolymers to inhibit heparanase activity could contribute synergistically to prevent cell adhesion and thus to tumor metastasis. Extensive structural studies have been performed to identify high binding heparin derivatives to heparanase,[42] which have been developed to heparin-derived drug candidates such as sulfated glycopolymers.[43,44] In line with those recently published compounds, the inhibitory activities obtained by both poly(SSS-*co*-AA) and poly(SPA-*co*-AA)-1:1 copolymers in the low nanomolar range are extremely promising and even exceed the clinical candidate for heparanase inhibition PG545 (Pixatimod). These motivating findings should be explored further for inhibition of tumor metastasis in animal models.

CONCLUSIONS

This is the first report on the activities of synthetic polymers as heparin mimetics in an oncological context. Our data provide an insight into the capacities of these synthetic polymers to interfere at different stages of the metastatic cascade of tumor cells, partly outmatching the activities of heparin or LMWH. These promising initial findings warrant further studies in this field to derive structure−activity relationships to better understand the yet not decoded activities of heparin in oncology, aiming to substitute heparin as nonideal drugs by defined and rationally designed synthetic analogues in the future.

EXPERIMENAL PROCEDURE

Cell Lines. Human breast cancer cell line MDA-MB-231 was cultivated in high-glucose Dulbecco's modified Eagle's medium (DMEM) supplemented with 10% FCS, 2 mM L-glutamine, 1 mM sodium pyruvate, 100 U/mL penicillin, and 100 μg/mL streptomycin (all from PAN Biotech, Aidenbach, Germany). MV3 wt cells were maintained in RPMI 1640 medium (PAN Biotech) supplemented with 10% FCS, 100 U/mL penicillin, and 100 μg/mL streptomycin. For cultivation of MV3-ITGB1, knockdown cells and their corresponding scramble control 1.5 μg/mL puromycin (Carl Roth GmbH+ Co.KG, Karlsruhe, Germany) were added to the medium. EA.hy926 endothelial cells were maintained in DMEM—low-glucose medium (Sigma-Aldrich Chemie GmbH, Steinheim, Germany) supplemented with 10% FCS, 100 U/mL penicillin, 100 μg/mL streptomycin (all from PAN Biotech), and 3.7 mg/mL $NaHCO_3$ (Sigma-Aldrich). Human umbilical vein endothelial cells (HUVECs) were cultured in two-thirds M199 supplemented with 10% heat-inactivated fetal calf serum, 1% antibiotics (penicillin and streptomycin), and one-third EGM-2 (Lonza Group AG, Basel, Switzerland). For subcultivation and assay application, cells were detached with 0.2 g/L EDTA × tetra sodium solution. Cells were maintained at 37 °C in a humidified atmosphere containing 5% CO_2. Cell lines were regularly tested for mycoplasma contamination. Cell lines were authenticated by the Leibniz-Institute DSMZ GmbH using nanoplex PCR to investigate Short Tandem Repeats.

Platelet Isolation. PRP was obtained from Institute for Experimental Hematology and Transfusion Medicine, University of Bonn, Medical Centre. Platelets were separated by

https://doi.org/10.1021/acsami.0c20744
ACS Appl. Mater. Interfaces 2021, 13, 7080−7093

centrifugation at 670*g*, RT for 10 min. The pellet was resuspended and adjusted to 4×10^8 platelets/mL in platelet buffer (10 mM HEPES, 140 mM NaCl, 3 mM KCl, 0.5 mM $MgCl_2$, 5 mM $NaHCO_3$, and 10 mM glucose). Platelet suspensions were supplemented with $CaCl_2$ at 1 mM final concentration and 0.5% plasma. Prior to activation, platelets were incubated with indicated test compounds for 30 min. Commercially available UFH (Ratiopharm GmbH, Ulm, Germany), enoxaparin (Sanofi-Aventis Deutschland GmbH, Frankfurt, Germany), and fondaparinux (Aspen Pharma Trading Ltd, Dublin, Ireland) were applied at adopted therapeutic concentrations of 1 IU/mL, 1 IU/mL, and 775 ng/mL, respectively. Heparin-mimicking polymers were applied at final concentrations of 50 and 600 μg/mL (thrombin generation assay).

Light Transmission Aggregometry. Platelet aggregation induced by tumor cells was assessed by LTA using an APACT 4004 aggregometer (Haemochrom Diagnostica GmbH, Essen, Germany). Platelet samples were prepared as mentioned before. Light transmission was measured continuously at 37 °C in cuvettes, stirring at 1000 rpm, to record kinetics of aggregate formation. As activating agents, either 1×10^4 MDA-MB-231 cells or 41.25 μM TRAP-6 (Cayman Chemical, Ann Arbor, MI, USA) were used. As benchmark for 0% aggregation, nonactivated platelets in platelet buffer and as 100% aggregation platelet buffer without platelets were applied.

Platelet Protein Release. The release of proteins stored in platelet granules was applied as a further marker for platelet activation. Therefore, platelets were isolated as mentioned above and were activated using a final concentration of 1×10^4 MDA-MB-231 cells per mL. After an incubation of 12 min, platelets were centrifuged at 10,000*g* at 4 °C for 10 min. Supernatants were collected and analyzed with the inflammation panel of the PEA by Olink Bioscience, Uppsala, Sweden.

ATP Assay. To quantify ATP release from platelets' dense granules, a luciferase-based ATP determination kit was used according to manufacturers' instructions (Thermo Fisher Scientific). Platelet samples were prepared as mentioned before and activated for 12 min with 1×10^4 MDA-MB-231 cells or 41.25 μM TRAP-6, respectively. Luminescence was measured using a Fluostar optima plate reader (BMG Labtech, Ortenberg, Germany). Results were normalized on the ATP release of TRAP-6-activated platelets.

Thrombin Generation Assay. Tumor cell-induced thrombin generation in human PRP was evaluated using a fluorogenic thrombin generation assay. To exclude thrombin formation by the intrinsic pathway, PRP was spiked with Corn Trypsin inhibitor (Santa Cruz Biotechnology, Santa Cruz, CA, USA) resulting in a concentration of 50 μg/mL. Afterward, PRP was incubated 30 min with the indicated compounds. Incubated samples were transferred to a 96-well plate and spiked with MDA-MB-231 cells resulting in a final concentration of 1×10^4 cells per mL. With addition of the substrate, reagent Technothrombin TGA SUB (Technoclone GmbH, Vienna, Austria) samples are recalcified and subsequently, thrombin-mediated Z-Gly-Gly-Arg-AMC cleavage was measured using the Fluoroskan Ascent reader (Thermo Fisher Scientific, Waltham, MA, USA). Fluorescence signals were converted to thrombin concentrations using the evaluation software provided by Technoclone GmbH. Integrity of PRP was tested by activation with the recombinant tissue factor reagent Technothrombin TGA RC high (Technoclone GmbH).

SAW Biosensor. SAW measurements were performed to extract kinetic constants of heparin mimetics binding to membrane-inserted P-selectin (Sino Biological Inc., Beijing, China) and VLA-4 (R&D systems, Minneapolis, USA). Analyses were performed using a Sam5 Blue SAW biosensor (SAW Instruments GmbH, Munich, Germany). For preparing a P-selectin or VLA-4 containing model membrane at the sensor surface, clean SAW sensor chips were preincubated for 12 h in a chloroform solution of 10 mM 1-hexadecanethiol to create a self-assembled monolayer on the vapor-deposited gold layer. After drying the quartz, a model membrane consisting of 20 mol % DGS-NTA (Ni) and 80 mol % DPPC (Sigma-Aldrich) was formed using the Langmuir–Blodgett technique and transferred to the sensors, as described before.[45] Therefore, the lipids were dissolved in the indicated ratio in chloroform and injected onto an aqueous phase in the Langmuir trough. After an equilibration time of 10 min, the lipid layer at the air/water interface was compressed to two-thirds of the collapse pressure. Subsequently, the sensor chips were vertically driven through the lipid layer. The membrane-coated sensors were subsequently incubated in an aqueous solution of 1.66 μM trehalose and dried overnight to allow a dry insertion of the intact model membrane into the measurement device. The dried membrane was reconstituted by starting the buffer flow (40 μL/min for baseline equilibration). Afterward, 2 μg rh His-tagged P-selectin or rh His-tagged VLA-4 was injected with a flow rate of 20 μL/min for binding of the protein polyhistidine tag to the DGS-NTA (Ni) lipid in the membrane. Subsequently, a dilution series of heparins or heparin mimetics between 5.2×10^{-10} and 8.32×10^{-6} M in running buffer (1 mM $CaCl_2$, 1 mM $MgCl_2$, and 0.5 mM $MnCl_2$) was injected for VLA-4 measurements. For P-selectin measurements, a dilution series between 5.2×10^{-9} and 6.76×10^{-6} M was injected. K_D, k_{on}, and k_{off} values were extracted from the binding curves using the SamBlue FitMaster software.

Flow Chamber Assay. A flow chamber assay was applied to evaluate the functional consequence of a VLA-4 binding by the heparins and heparin-mimicking polymers. Thus, the melanoma cells MV3 wt and MV3 scramble, both expressing VLA-4, as well as MV3-ITGB1 knockdown cells, were investigated for their adherence to immobilized VCAM-1 under physiological shear stress conditions as already described.[37] Glass slides (Ø 18 mm) were cleaned in a mixture of 15 mL of 30% H_2O_2 and 35 mL of H_2SO_4 concn with ultrasonication at 80 °C for 30 min. After washing the slides with Aqua dem., glass slides were cleaned in a mixture of 50 mL of Aqua dem., 10 mL of 30% H_2O_2, and 10 mL of 26% NH_3 with ultrasonication at 80 °C for 30 min. After washing with Aqua dem., the slides were dried at 80 °C. Cyanuric chloride was dissolved in anhydrous chloroform and glass slides were incubated for 30 min applying ultrasonication. Subsequently, the slides were washed for 20 min with ultrasonication in anhydrous chloroform. A total of 0.2 μg of VCAM-1 Fc chimera (BioLegend, San Diego, USA) in 80 μL of immobilization buffer [0.5% bovine serum albumin (BSA), 0.1 M boric acid in Aqua dem. pH 8.8] was placed on a dry slide and incubated at 4 °C for 12 h. The glass slides were mounted into the parallel flow chamber and placed on an inverted microscope. A shear rate of about 200 s^{-1} was set by hydrostatic pressure. For the experiments, MV3 cells were suspended in FCS-free medium. To stimulate VCAM-1/VLA-4 binding, cells were treated with 1 mM Mn^{2+} for 5 min at 37

https://doi.org/10.1021/acsami.0c20744
ACS Appl. Mater. Interfaces 2021, 13, 7080–7093

°C. For inhibitory experiments, the cells were simultaneously treated with the indicated concentrations of the compounds. A total of 7.5 × 10^5 MV3 cells were injected into the flow chamber and were allowed to bind to VCAM-1 for 5 min. Video sequences were captured with the CSC-795 camera (Pacific Corporation, Tokyo, Japan). Adhesive cells were monitored every 3 s.

Artificial Blood Vessels. To analyze the adhesion of blood flowing MV3 melanoma cells, we performed experiments in artificial blood vessels as previously reported.[46,47] Briefly, 5 × 10^5 HUVECs were seeded on gelatin-coated μ-slides 0.2 Luer (IBIDI GmbH, Munich, Germany) and cultivated in medium composed of two-thirds M199 supplemented with 10% heat-inactivated fetal calf serum, 1% antibiotics (penicillin and streptomycin), and one-third EGM-2 (Lonza Group AG, Basel, Switzerland) for 48 h at 37 °C and 5% CO_2. Prior to the flow experiments, HUVECs were stimulated with 10 ng/mL tumor necrosis factor-α for 4 h and labeled with a CD31-directed antibody CD31 (mouse anti-human monoclonal antibody, Agilent Dako, dilution 1:150) and the corresponding secondary antibodies conjugated with Alexa Fluor 647 (Thermo Fisher Scientific, Waltham, USA, dilution 1:1000). Human hirudin blood was spiked with 1 × 10^6 green fluorescent protein labeled and $MnCl_2$ (1 mM)-treated MV3 cells. Where indicated, MV3 cells were additionally treated with 50 μg/mL poly(SSS-*co*-AA)-1:1 20 kDa, 50 μg/mL poly(SPA-*co*-AA)-1:1 20 kDa, or 1 I.E./mL enoxaparin. Perfusion of the HUVECs with the blood was performed with a shear stress of 2 dyne/cm^2 for 30 min and adherent cells were imaged with a 20× objective mounted to an Observer Z.1 (Carl Zeiss AG, Jena, Germany). Data were processed with Zen software version 1.1.2.0 (Zeiss) and ImageJ (1.50c). Adhesion of MV3 cells was calculated as the product of the MV3 covered area and the fluorescence intensity of the cell or the cell clusters. For comparison of independent experiments, control slides (only $MgCl_2$ treatment) were normalized to 100% and MV3 adhesion is stated relatively.

Heparanase Enzymatic Activity Assay. Heparanase activity was determined using homogeneous time-resolved fluorescence (HTRF), a time-resolved fluorescence energy transfer-based assay, essentially following the instruction of the manufacturer (Cisbio Bioassays S.A.S., Codolet, France) after optimization. Heparanase was partially purified from the liver of transgenic mice overexpressing human heparanase.[48] All test compounds were dissolved and diluted to different concentrations using sample buffer (50 mM Tris−HCl pH 7.4, 0.15 M NaCl, 0.1% protease free BSA, 0.1% CHAPS). The compounds (3 μL) were mixed with 7 μL of heparanase in 384-well low-volume microplate. After 10 min preincubation at 37°, the enzyme reaction was initiated by adding 4.2 ng of Biotin-HS-Eu (substrate) in 5 μL of 0.2 M acetate buffer pH 5.5 to each well, and the plate was incubated for 30 min at 37°. Then, 12 ng of streptavidin-d2 acceptor (5 μL buffer of 62.5 mM Hepes pH 7.4, 0.8 M KF, 0.1% protease free BSA, 2 mg/mL heparin) was added to stop the reaction. After 15 min incubation at RT, the enzyme activity was detected by determining the HTRF signal ratio of 665/620 nm in a FLUOstar OMEGA reader (BMG Labtech). Each reaction was run in triplicate.

Statistical Analysis. Data represent means ± standard deviations. If not stated otherwise in the figure legends, experiments were performed in three independent replicates (N = 3). GraphPad Prism Version 6 was used to perform Student's t-test for statistical analysis. *: $p < 0.05$; **: $p < 0.01$; and ***: $p < 0.001$.

■ ASSOCIATED CONTENT

Supporting Information

The Supporting Information is available free of charge at https://pubs.acs.org/doi/10.1021/acsami.0c20744.

Representative curves of LTA screening, extracted peak thrombin values from TGA, extracted ETP values from TGA, cell cytotoxicity data EA.hy926, and dispersities of the applied polymers (PDF)

■ AUTHOR INFORMATION

Corresponding Author

Gerd Bendas − *Pharmaceutical Institute, Pharmaceutical and Cell Biological Chemistry, University of Bonn, 53121 Bonn, Germany;* orcid.org/0000-0002-8667-7201; Email: gbendas@uni-bonn.de

Authors

Lukas M. Gockel − *Pharmaceutical Institute, Pharmaceutical and Cell Biological Chemistry, University of Bonn, 53121 Bonn, Germany*

Martin Heyes − *Pharmaceutical Institute, Pharmaceutical and Cell Biological Chemistry, University of Bonn, 53121 Bonn, Germany*

Honglian Li − *Department of Medical Biochemistry and Microbiology, SciLifeLab Uppsala, The Biomedical Center, University of Uppsala, 75123 Uppsala, Sweden*

Abdullah Al Nahain − *School of Chemistry and Molecular Biosciences and Australian Infectious Diseases Research Centre, The University of Queensland, Brisbane, Queensland 4072, Australia*

Christian Gorzelanny − *Experimental Dermatology, Department of Dermatology and Venereology, University Medical Center Hamburg-Eppendorf, 20246 Hamburg, Germany*

Martin Schlesinger − *Pharmaceutical Institute, Pharmaceutical and Cell Biological Chemistry, University of Bonn, 53121 Bonn, Germany*

Stefan Holdenrieder − *The German Heart Centre of Technical University Munich, Laboratory Medicine, 80636 Munich, Germany*

Jin-Ping Li − *Department of Medical Biochemistry and Microbiology, SciLifeLab Uppsala, The Biomedical Center, University of Uppsala, 75123 Uppsala, Sweden*

Vito Ferro − *School of Chemistry and Molecular Biosciences and Australian Infectious Diseases Research Centre, The University of Queensland, Brisbane, Queensland 4072, Australia;* orcid.org/0000-0003-3306-2550

Complete contact information is available at: https://pubs.acs.org/10.1021/acsami.0c20744

Author Contributions

Conceptualization, G.B. and V.F.; Methodology, M.S., S.H., V.F., G.B., and J.-P.L.; Investigation, L.M.G., M.H., C.G., and H.L.; Resources, A.A.N., V.F., G.B., and S.H.; Compound Synthesis, A.A.N. and V.F.; Writing-Original Draft, L.M.G., M.S., and G.B.; Writing-Review and Editing, V.F., J.-P.L., and S.H.; Visualization, L.M.G., H.L., and M.H.; and Supervision, G.B.

Notes

The authors declare no competing financial interest.

■ ACKNOWLEDGMENTS

V.F. gratefully acknowledges support from the Australian Research Council (DP170104431), J.-P.L. acknowledges a grant support by the Swedish Cancer Foundation (CAN2018/541), and C.G. acknowledges the support from the Erich and Gertrud Roggenbuck foundation. The authors would like to thank Prof. J. Oldenburg and E. Hanfland, Institute for Experimental Hematology and Transfusion Medicine, University of Bonn, for their support in providing human platelet preparations.

■ ABBREVIATIONS

AA, acrylic acid
AMPS, sodium-2-acrylamido-2-methyl-1-propane sulfonate
APTT, activated partial thromboplastin time
Đ, dispersity
GAG, glycosaminoglycan
HGF, hepatocyte growth factor
HS, heparan sulfate
K_D, dissociation constant
k_{off}, dissociation rate constant
k_{on}, association rate constant
LAP, latency-associated peptide
LMWH, low-molecular-weight heparin
LTA, light transmission aggregometry
MCP-1, monocyte chemoattractant protein-1
MMP-1, matrix metalloproteinase-1
n.d., not detectable
PAR, protease-activated receptor
PRP, platelet-rich plasma
RAFT, reversible addition−fragmentation chain transfer
SPA, potassium-3-sulfopropyl acrylate
SPM, potassium-3-sulfopropyl methacrylate
SSS, sodium 4-styrenesulfonate
TCIPA, tumor cell-induced platelet activation
TCT, thrombin clotting time
TGF, transforming growth factor
UFH, unfractionated heparin
VCAM-1, vascular cell adhesion molecule 1
VEGF, vascular endothelial growth factor
VLA-4, very late antigen-4

■ REFERENCES

(1) GBD 2017 Causes of Death Collaborators. Global, regional, and national age-sex-specific mortality for 282 causes of death in 195 countries and territories, 1980-2017: a systematic analysis for the Global Burden of Disease Study 2017. *Lancet* **2018**, *392*, 1736−1788.
(2) Dillekås, H.; Rogers, M. S.; Straume, O. Are 90% of Deaths from Cancer Caused by Metastases? *Cancer Med.* **2019**, *8*, 5574−5576.
(3) Dickmann, B.; Ahlbrecht, J.; Ay, C.; Dunkler, D.; Thaler, J.; Scheithauer, W.; Quehenberger, P.; Zielinski, C.; Pabinger, I. Regional Lymph Node Metastases Are a Strong Risk Factor for Venous Thromboembolism: Results from the Vienna Cancer and Thrombosis Study. *Haematologica* **2013**, *98*, 1309−1314.
(4) Wun, T.; White, R. H. Epidemiology of Cancer-Related Venous Thromboembolism. *Best Pract. Res., Clin. Haematol.* **2009**, *22*, 9−23.
(5) Varki, A. Trousseau's Syndrome: Multiple Definitions and Multiple Mechanisms. *Blood* **2007**, *110*, 1723−1729.
(6) Oppelt, P.; Betbadal, A.; Nayak, L. Approach to Chemotherapy-Associated Thrombosis. *Vasc. Med.* **2015**, *20*, 153−161.
(7) Walker, A. J.; Card, T. R.; West, J.; Crooks, C.; Grainge, M. J. Incidence of Venous Thromboembolism in Patients with Cancer − A Cohort Study Using Linked United Kingdom Databases. *Eur. J. Cancer* **2013**, *49*, 1404−1413.
(8) Khorana, A. A. Venous Thromboembolism and Prognosis in Cancer. *Thromb. Res.* **2010**, *125*, 490−493.
(9) Sørensen, H. T.; Mellemkjær, L.; Olsen, J. H.; Baron, J. A. Prognosis of Cancers Associated with Venous Thromboembolism. *N. Engl. J. Med.* **2000**, *343*, 1846−1850.
(10) Farge, D.; Frere, C.; Connors, J. M.; Ay, C.; Khorana, A. A.; Munoz, A.; Brenner, B.; Kakkar, A.; Rafii, H.; Solymoss, S.; Brilhante, D.; Monreal, M.; Bounameaux, H.; Pabinger, I.; Douketis, J.; Ageno, W.; Ajauro, F.; Al-Aboudi, K. R.; Alcindor, T.; Andre, T.; Angchaisuksiri, P.; Antic, D.; Arcelus, J. I.; Assenat, E.; Bauer, K. A.; Bazarbachii, A.; Benzidia, I.; Beyer-Westendorf, J.; Bitsadze, V.; Blickstein, D.; Blostein, M.; Bogalho, I.; Bournet, B.; Casais, P.; Carpentier, A. F.; Cesarman-Maus, G.; Chakbrabartty, J.; Clemente, H.; Connault, J.; Doucet, L.; Durant, C.; Emmerich, J.; Falanga, A.; Feistritzer, C.; Font, C.; Francis, C.; Gallardo, E.; Gary, T.; Gris, J.-C.; Guillermo, C.; Hij, A.; Hull, R. D.; IKezoe, T.; Jara-Palomares, L.; Key, N. S.; Khrizroeva, J.; Koolian, M.; Langer, F.; Le Hello, C.; Lecumberri, R.; Lee, L. H.; Liebman, H.; Lopes Dos Santos, L.; Machado, D. H.; Madelaine, I.; Makatsariya, A.; Mandala, M.; Marayevas, A.; Marjanovic, Z.; Marosi, C.; Martin, E.; Meillon, L.; Messas, E.; Moreira, A.; Demir, A. M.; Ndour, A.; Nguessan, M.; Otero-Candelera, R.; Pachon Olmos, V.; Pais, A.; Posch, F.; Preusser, M.; Riess, H.; Righini, M.; Rothschild, C.; Roussin, A.; Rueda-Camino, J. A.; Ruiz-Artacho, P.; Saseedharan, S.; Shamseddine, A.; Soff, G.; Stricker, H.; Tagalakis, V.; Taher, A.; Toussaint, T.; Trujillo-Santos, J.; Villiers, S.; Wong, R.; Yamada, N. 2019 International Clinical Practice Guidelines for the Treatment and Prophylaxis of Venous Thromboembolism in Patients with Cancer. *Lancet Oncol.* **2019**, *20*, e566−e581.
(11) Ek, L.; Gezelius, E.; Bergman, B.; Bendahl, P. O.; Anderson, H.; Sundberg, J.; Wallberg, M.; Falkmer, U.; Verma, S.; Belting, M.; Swedish Lung Cancer Study Group (SLUSG). Randomized Phase III Trial of Low-Molecular-Weight Heparin Enoxaparin in Addition to Standard Treatment in Small-Cell Lung Cancer: The RASTEN Trial. *Ann. Oncol.* **2018**, *29*, 398−404.
(12) Kakkar, A. K.; Levine, M. N.; Kadziola, Z.; Lemoine, N. R.; Low, V.; Patel, H. K.; Rustin, G.; Thomas, M.; Quigley, M.; Williamson, R. C. N. Low Molecular Weight Heparin, Therapy With Dalteparin, and Survival in Advanced Cancer: The Fragmin Advanced Malignancy Outcome Study (FAMOUS). *J. Clin. Oncol.* **2004**, *22*, 1944−1948.
(13) Borsig, L.; Wong, R.; Hynes, R. O.; Varki, N. M.; Varki, A. Synergistic Effects of L- and P-Selectin in Facilitating Tumor Metastasis Can Involve Non-Mucin Ligands and Implicate Leukocytes as Enhancers of Metastasis. *Proc. Natl. Acad. Sci. U.S.A.* **2002**, *99*, 2193−2198.
(14) Fritzsche, J.; Simonis, D.; Bendas, G. Melanoma Cell Adhesion Can Be Blocked by Heparin in Vitro: Suggestion of VLA-4 as a Novel Target for Antimetastatic Approaches. *Thromb. Haemostasis* **2008**, *100*, 1166−1175.
(15) Zhang, C.; Liu, Y.; Gao, Y.; Shen, J.; Zheng, S.; Wei, M.; Zeng, X. Modified Heparins Inhibit Integrin $\alpha_{IIb}\beta_3$ Mediated Adhesion of Melanoma Cells to Platelets in Vitro and in Vivo. *Int. J. Cancer* **2009**, *125*, 2058−2065.
(16) Vlodavsky, I.; Abboud-Jarrous, G.; Elkin, M.; Naggi, A.; Casu, B.; Sasisekharan, R.; Ilan, N. The Impact of Heparanase and Heparin on Cancer Metastasis and Angiogenesis. *Pathophysiol. Haemostasis Thromb.* **2006**, *35*, 116−127.
(17) Ornstein, D. L.; Zacharski, L. R. The Use of Heparin for Treating Human Malignancies. *Pathophysiol. Haemostasis Thromb.* **1999**, *29*, 48−60.
(18) Mohamed, S.; Coombe, D. Heparin Mimetics: Their Therapeutic Potential. *Pharmaceuticals* **2017**, *10*, 78.

https://doi.org/10.1021/acsami.0c20744
ACS Appl. Mater. Interfaces 2021, 13, 7080−7093

(19) Erpenbeck, L.; Schön, M. P. Deadly Allies: The Fatal Interplay between Platelets and Metastasizing Cancer Cells. *Blood* **2010**, *115*, 3427−3436.
(20) Goubran, H.; Stakiw, J.; Radosevic, M.; Burnouf, T. Platelet−Cancer Interactions. *Semin. Thromb. Hemostasis* **2014**, *40*, 296−305.
(21) Gockel, L.; Ponert, J.; Schwarz, S.; Schlesinger, M.; Bendas, G. The Low Molecular Weight Heparin Tinzaparin Attenuates Platelet Activation in Terms of Metastatic Niche Formation by Coagulation-Dependent and Independent Pathways. *Molecules* **2018**, *23*, 2753.
(22) Schwarz, S.; Gockel, L. M.; Naggi, A.; Barash, U.; Gobec, M.; Bendas, G.; Schlesinger, M. Glycosaminoglycans as Tools to Decipher the Platelet Tumor Cell Interaction: A Focus on P-Selectin. *Molecules* **2020**, *25*, 1039.
(23) Zhu, Y.; Zhang, F.; Linhardt, R. J. Heparin Contamination and Issues Related to Raw Materials and Controls. In *The Science and Regulations of Naturally Derived Complex Drugs*; Sasisekharan, R., Lee, S. L., Rosenberg, A., Walker, L. A., Eds.; AAPS Advances in the Pharmaceutical Sciences Series; Springer International Publishing: Cham, 2019; Vol. *32*, pp 191−206.
(24) Arepally, G. M. Heparin-Induced Thrombocytopenia. *Blood* **2017**, *129*, 2864−2872.
(25) Bussey, H.; Francis, J. L.; Consensus Group, T. H. Heparin Overview and Issues. *Pharmacotherapy* **2004**, *24*, 103S−107S.
(26) Nahain, A. A.; Ignjatovic, V.; Monagle, P.; Tsanaktsidis, J.; Ferro, V. Heparin Mimetics with Anticoagulant Activity. *Med. Res. Rev.* **2018**, *38*, 1582−1613.
(27) Paluck, S. J.; Nguyen, T. H.; Maynard, H. D. Heparin-Mimicking Polymers: Synthesis and Biological Applications. *Biomacromolecules* **2016**, *17*, 3417−3440.
(28) Oh, Y. I.; Sheng, G. J.; Chang, S.-K.; Hsieh-Wilson, L. C. Tailored Glycopolymers as Anticoagulant Heparin Mimetics. *Angew. Chem., Int. Ed.* **2013**, *52*, 11796−11799.
(29) Nahain, A. A.; Ignjatovic, V.; Monagle, P.; Tsanaktsidis, J.; Vamvounis, G.; Ferro, V. Anticoagulant Heparin Mimetics via RAFT Polymerization. *Biomacromolecules* **2020**, *21*, 1009−1021.
(30) Nahain, A. A.; Ignjatovic, V.; Monagle, P.; Tsanaktsidis, J.; Vamvounis, G.; Ferro, V. Sulfonated RAFT Copolymers as Heparin Mimetics: Synthesis, Reactivity Ratios, and Anticoagulant Activity. *Macromol. Biosci.* **2020**, *20*, 2000110.
(31) Ma, S.-N.; Mao, Z.-X.; Wu, Y.; Liang, M.-X.; Wang, D.-D.; Chen, X.; Chang, P.-a.; Zhang, W.; Tang, J.-H. The Anti-Cancer Properties of Heparin and Its Derivatives: A Review and Prospect. *Cell Adhes. Migr.* **2020**, *14*, 118−128.
(32) Gay, L. J.; Felding-Habermann, B. Contribution of Platelets to Tumour Metastasis. *Nat. Rev. Cancer* **2011**, *11*, 123−134.
(33) Wojtukiewicz, M. Z.; Hempel, D.; Sierko, E.; Tucker, S. C.; Honn, K. V. Thrombin—Unique Coagulation System Protein with Multifaceted Impacts on Cancer and Metastasis. *Cancer Metastasis Rev.* **2016**, *35*, 213−233.
(34) Ludwig, R. J.; Boehme, B.; Podda, M.; Henschler, R.; Jager, E.; Tandi, C.; Boehncke, W.-H.; Zollner, T. M.; Kaufmann, R.; Gille, J. Endothelial P-Selectin as a Target of Heparin Action in Experimental Melanoma Lung Metastasis. *Cancer Res.* **2004**, *64*, 2743−2750.
(35) Wang, J.-G.; Geng, J.-G. Affinity and Kinetics of P-Selectin Binding to Heparin. *Thromb. Haemostasis* **2003**, *90*, 309−316.
(36) Simonis, D.; Fritzsche, J.; Alban, S.; Bendas, G. Kinetic Analysis of Heparin and Glucan Sulfates Binding to P-Selectin and Its Impact on the General Understanding of Selectin Inhibition †. *Biochemistry* **2007**, *46*, 6156−6164.
(37) Schlesinger, M.; Simonis, D.; Schmitz, P.; Fritzsche, J.; Bendas, G. Binding between Heparin and the Integrin VLA-4. *Thromb. Haemostasis* **2009**, *102*, 816−822.
(38) Casu, B.; Vlodavsky, I.; Sanderson, R. D. Non-Anticoagulant Heparins and Inhibition of Cancer. *Pathophysiol. Haemostasis Thromb.* **2007**, *36*, 195−203.
(39) Schlesinger, M.; Bendas, G. Contribution of Very Late Antigen-4 (VLA-4) Integrin to Cancer Progression and Metastasis. *Cancer Metastasis Rev.* **2015**, *34*, 575−591.
(40) Vlodavsky, I.; Singh, P.; Boyango, I.; Gutter-Kapon, L.; Elkin, M.; Sanderson, R. D.; Ilan, N. Heparanase: From Basic Research to Therapeutic Applications in Cancer and Inflammation. *Drug Resist. Updates* **2016**, *29*, 54−75.
(41) Zhang, G.-L.; Gutter-Kapon, L.; Ilan, N.; Batool, T.; Singh, K.; Digre, A.; Luo, Z.; Sandler, S.; Shaked, Y.; Sanderson, R. D.; Wang, X.-M.; Li, J.-P.; Vlodavsky, I. Significance of Host Heparanase in Promoting Tumor Growth and Metastasis. *Matrix Biol.* **2020**, *93*, 25.
(42) Bendas, G.; Borsig, L. Heparanase in Cancer Metastasis − Heparin as a Potential Inhibitor of Cell Adhesion Molecules. In *Heparanase*; Vlodavsky, I., Sanderson, R. D., Ilan, N., Eds.; Advances in Experimental Medicine and Biology; Springer International Publishing: Cham, 2020; Vol. *1221*, pp 309−329.
(43) Loka, R. S.; Sletten, E. T.; Barash, U.; Vlodavsky, I.; Nguyen, H. M. Specific Inhibition of Heparanase by a Glycopolymer with Well-Defined Sulfation Pattern Prevents Breast Cancer Metastasis in Mice. *ACS Appl. Mater. Interfaces* **2019**, *11*, 244−254.
(44) Zubkova, O. V.; Ahmed, Y. A.; Guimond, S. E.; Noble, S.-L.; Miller, J. H.; Alfred Smith, R. A.; Nurcombe, V.; Tyler, P. C.; Weissmann, M.; Vlodavsky, I.; Turnbull, J. E. Dendrimer Heparan Sulfate Glycomimetics: Potent Heparanase Inhibitors for Anticancer Therapy. *ACS Chem. Biol.* **2018**, *13*, 3236−3242.
(45) Reder-Christ, K.; Schmitz, P.; Bota, M.; Gerber, U.; Falkenstein-Paul, H.; Fuss, C.; Enachescu, M.; Bendas, G. A Dry Membrane Protection Technique to Allow Surface Acoustic Wave Biosensor Measurements of Biological Model Membrane Approaches. *Sensors* **2013**, *13*, 12392−12405.
(46) John, A.; Günes, C.; Bolenz, C.; Vidal-y-Sy, S.; Bauer, A. T.; Schneider, S. W.; Gorzelanny, C. Bladder Cancer-Derived Interleukin-1 Converts the Vascular Endothelium into a pro-Inflammatory and pro-Coagulatory Surface. *BMC Cancer* **2020**, *20*, 1178.
(47) Kalagara, T.; Moutsis, T.; Yang, Y.; Pappelbaum, K. I.; Farken, A.; Cladder-Micus, L.; Vidal-y-Sy, S.; John, A.; Bauer, A. T.; Moerschbacher, B. M.; Schneider, S. W.; Gorzelanny, C. The Endothelial Glycocalyx Anchors von Willebrand Factor Fibers to the Vascular Endothelium. *Blood Adv.* **2018**, *2*, 2347−2357.
(48) Zcharia, E.; Metzger, S.; Chajek-Shaul, T.; Aingorn, H.; Elkin, M.; Friedmann, Y.; Weinstein, T.; Li, J. P.; Lindahl, U.; Vlodavsky, I. Transgenic Expression of Mammalian Heparanase Uncovers Physiological Functions of Heparan Sulfate in Tissue Morphogenesis, Vascularization, and Feeding Behavior. *FASEB J.* **2004**, *18*, 252−263.

NOTE ADDED AFTER ISSUE PUBLICATION

This article was initially published with an incorrect copyright statement and was corrected on or around May 5, 2021.

https://doi.org/10.1021/acsami.0c20744
ACS Appl. Mater. Interfaces 2021, 13, 7080−7093